Structural Perturbations in Human ADP Ribosylation Factor-1 Accompanying the Binding of Phosphatidylinositides†

Ronald D. Seidel, III,‡ Juan Carlos Amor,§ Richard A. Kahn,§ and James H. Prestegard*,‡

Complex Carbohydrate Research Center, University of Georgia, 315 Riverbend Road, Athens, Georgia 30602-4712, and Department of Biochemistry, Emory University School of Medicine, 1510 Clifton Road, Atlanta, Georgia 30322-3050

Received May 12, 2004; Revised Manuscript Received September 13, 2004

ABSTRACT: ADP ribosylation factors (Arfs) are members of a family of Ras-related GTPases that regulate a wide variety of intracellular signaling pathways, including the regulation of membrane traffic and organelle morphology. Arfs perform these functions through interactions with Arf-specific guanine nucleotide exchange factors (GEFs), GTPase activating proteins (GAPs), and effectors. Signaling phosphatidylinositides, most commonly phosphatidylinositol (4,5)-bisphosphate ($PI(4,5)P_2$) or phosphatidylinositol (3,4,5)-trisphosphate ($PI(3,4,5)P_3$), have been shown previously to regulate the activities of a number of these regulators and effectors of Arf. The ability of Arf itself to bind these same phosphatidylinositides also has been reported previously, though without much structural detail. We investigated the ability of human Arf1·GDP (Arf1·GDP) to bind myo-inositol (1,4,5)-trisphosphate ($I(1,4,5)P_3$), the soluble headgroup for $PI(4,5)P_2$, and a short acyl-chain soluble $PI(4,5)P_2$ analogue using heteronuclear single quantum coherence (HSQC)-based NMR techniques. A patch of positive electrostatic potential on the surface of Arf1·GDP is identified as being directly involved in ligand binding, but structural and stability changes extending to the N-terminal helix and nucleotide-binding site of Arf1 are also documented. The identified binding site and the resultant structural changes are discussed in terms of a possible influence of phosphatidylinositides on the binding of Arf1 to Arf1-GEF and subsequent nucleotide release.

ADP ribosylation factors (Arfs) are a family of ∼21 kDa guanine nucleotide-binding proteins that are ubiquitously expressed in eukaryotic cells. Their best-characterized roles include regulation of a wide variety of intracellular signaling pathways such as membrane traffic and organelle structure at the Golgi, trans-Golgi network, endosomes, and the plasma membrane. Indispensable to the actions of Arfs in vivo is their ability to reversibly bind to biological membranes on which they encounter both their effectors and regulators, including the activating guanine nucleotide exchange factors (GEFs)[1] and signal-terminating GTPase activating proteins (GAPs) (*1*, *2*). Interactions with a subset of each are in turn regulated by the lipid composition, specifically by the presence of different phosphoinositides (e.g., phosphatidylinositol (4,5)-bisphosphate ($PI(4,5)P_2$) or phosphatidylinositol (3,4,5)-trisphosphate ($PI(3,4,5)P_3$) (*3*).

The ability of Arf itself to bind phosphoinositides was first predicted from the presence of a "positive patch" on the surface of the protein structure (*4*). The importance of this patch was confirmed by observations that mutation of the lysines and arginines in this polybasic domain resulted in alterations in lipid interactions and the lipid requirements for GAP-stimulated hydrolysis of Arf-bound GDP (*5*). In contrast to the role of phosphoinositides as required cofactors, for example, in the Arf-stimulated activation of phospholipase D (*6*, *7*) or Arf GAP activities (*8*), $PI(4,5)P_2$ has the ability to independently promote the release of GDP from Arf1 in vitro and stabilize the apoprotein (*9*, *10*), thus potentially acting as an Arf GEF. Additional evidence supporting a direct functional role for the interaction of phosphoinositides with Arf comes from the observation that nucleotide exchange stimulated by phosphoinositide-dependent GEFs is still present upon removal of the membrane recruitment domain of the exchange factor (*2*). Hence, there is evidence for the functional importance of phosphoinositide interactions with Arf but few details on the structural changes that accompany the interactions between these lipids and Arfs.

We have now investigated the ability of nonmyristoylated Arf1·GDP (Arf1·GDP) to bind soluble $PI(4,5)P_2$ analogues using $^{15}N-^{1}H$ heteronuclear single quantum coherence (HSQC)-based NMR experiments. HSQC experiments are ideally suited for resolving local structural variation accompanying ligand binding due to the innate ability to separate individual amino acid resonances based on their electronic environment. Cross-peaks in these spectra appear

† This work is supported by the National Institutes of Health, Grant Number GM61268.

* To whom correspondence should be addressed. E-mail: jpresteg@ccrc.uga.edu. Phone: 706-542-6281. Fax: 706-542-4412.

‡ University of Georgia.

§ Emory University School of Medicine.

[1] Abbreviations: Arf1, human ADP-ribosylation factor 1; GAP, GTPase activating protein; GDP, guanosine 5′-diphosphate; GEF, guanine nucleotide exchange factor; GTP, guanosine 5′-triphosphate; HSQC, heteronuclear single quantum coherence; $I(1,4,5)P_3$, myo-inositol (1,4,5)-trisphosphate; myoI, D-myo-inositol; myoI-(1)P, D-myo-inositol (1)-monophosphate; myoI-$(1,4)P_2$, D-myo-inositol (1,4)-bisphosphate; myoI-$(4,5)P_2$, D-myo-inositol (4,5)-bisphosphate; NMR, nuclear magnetic resonance; $PI(4,5)P_2$, phosphatidylinositol (4,5)-bisphosphate; $PI(3,4,5)P_3$, phosphatidylinositol (3,4,5)-trisphosphate; TEMPOL, 4-hydroxy-2,2,6,6-tetramethyl-piperidine-1-oxyl.

10.1021/bi0490385 CCC: $27.50
Published on Web 11/17/2004

at positions that correlate amide proton chemical shifts with amide nitrogen chemical shifts. Changes in local environment are then reflected in differences in cross-peak positions between spectra of protein and those of protein−ligand complexes (*11*, *12*). In the current study, we have examined the ability of Arf1·GDP to bind to myo-inositol (1,4,5)-trisphosphate ($I(1,4,5)P_3$), the soluble headgroup found in phosphatidylinositol (4,5)-bisphosphate ($PI(4,5)P_2$), as well as a soluble, short acyl chain $PI(4,5)P_2$ analogue, using HSQC-based NMR experiments. With use of the previously determined $^{15}N-^{1}H$ backbone assignments on Arf1·GDP (*13*), selective changes in chemical shifts for certain resonances of these protein−ligand complexes were used both to map a putative binding pocket within Arf1·GDP and to measure relative binding affinities for some of the ligands.

Chemical shift changes are sometimes not confined to a single region of the protein. When this occurs, making a distinction among effects from ligand binding at one site, ligand binging at multiple sites, and structural changes induced at remotes sites is often difficult. However, distinction can be achieved by combining shift perturbation experiments with a number of other NMR-based techniques. One class of experiment that can contribute to a distinction relies on the direct protection of surface residues from spin relaxation enhancement by a soluble paramagnetic agent (*14*). Enhanced relaxation in the presence of such an agent is easily seen via a loss in intensity for HSQC peaks from protected residues. TEMPOL provides a neutral, soluble agent that will not be directly affected by electrostatic changes on binding of the highly charged ligands to be investigated. Monitoring changes in amide proton exchange rates upon ligand binding (*15*) can further substantiate the nature of changes induced directly at ligand binding sites or indirectly at remote sites. The more rapidly exchanging amides likely to be involved in these sites are easily monitored through experiments in which peak intensities depend on magnetization from water protons that exchange into the sites (CLEANEX experiments, *16*). Altered rates of magnetization transfer can reflect changes in stability of structural elements at various sites. Such stability changes may be particularly important in promoting nucleotide release and Arf−GEF associations needed for Arf activation.

Raising the possibility that phosphoinositide binding may induce more remote conformational changes is not without basis. It has been suggested, for example, that some of the conformational changes within Arf1 needed for activation and GTP binding occur prior to GDP release and upon interaction of Arf1 with its corresponding GEF on the membrane surface (*1*). These membrane-induced changes could well be mediated by specific interactions with phosphoinositides. While several structures have been described for Arf bound to a GEF or GAP, there is currently no direct structural information on Arf binding to a lipid or a membrane. We hope to provide a step toward resolving this deficiency with the studies of phosphoinositide binding that follow.

MATERIALS AND METHODS

Sample Preparation and Effector Selection. Human Arf1 was expressed in BL21(DE3) as previously described (*17*) but with modifications to allow the incorporation of stable isotopes. Transformed cells were grown to saturation in 3 mL of LB/Amp, collected, and placed in 50 mL of LB/Amp media and grown to an OD_{600} of 0.6. Cells were then collected and placed into 1 L of MOPS/Amp media (*18*) supplemented with 1× GIBCO vitamin mix (cat. no. 11120-052), 1 g/L $^{15}NH_4Cl$ and 4 g/L glucose. At an OD_{600} of 1.0, protein expression was induced by the addition of isopropyl-β-D-thiogalactopyranoside (IPTG) to 0.5 mM. After 3−5 h, cells were collected, resuspended in 10 mL of TM buffer (20 mM Tris, 2 mM $MgCl_2$, pH 7.6, at room temperature (RT)) and lysed using a French press. Cell lysate was clarified by centrifugation at 100 000 × *g* for 1 hr.

Soluble Arf1 was purified in two chromatographic steps, as previously described (*17*). A Q-macro resin column (BioRad, high-substitution; 50 mL bed volume) was equilibrated in TM buffer (20 mM Tris, 2 mM $MgCl_2$, pH 7.6, at RT), and proteins were resolved with a NaCl gradient. Fractions containing Arf1 were pooled, concentrated to 0.5 mL, and loaded onto a Superdex75 gel filtration column (Amersham; 60 cm × 1.6 cm) at a flow rate of 1.0 mL/min in phosphate buffer (10 mM KPO_4, 50 mM NaCl, 1 mM $MgCl_2$, and 5 mM NaN_3, pH 7.0, at RT). These conditions have been selected to allow for accurate transfer of $^{15}N-^{1}H$ assignments as previously collected (*13*).

Samples for titration experiments were 0.5 mM Arf1·GDP in the phosphate buffer with 10% $^{2}H_2O$ added to provide a lock signal. Due to low ligand volumes, data collection proceeded using either a 300 μL sample in a 5 mm (inner diameter) Shigemi tube (myoI, myoI-(1)P, myoI-$(1,4)P_2$, or $I(1,4,5)P_3$) or a 200 μL sample in a 3 mm Shigemi tube (myoI-$(4,5)P_2$ and dibutyryl-$PI(4,5)P_2$ (0.3 mM Arf1)). When solubility allowed, binding of effectors was monitored in 0.25 mM increments at concentrations ranging from 0 to 10 mM effector. NMR samples for separation of pH-induced shifts were 1.0 mM Arf1·GDP in the same buffer with pH values ranging from pH 6.0 to 7.0 in 0.25 unit steps.

The choice of phosphoinositide analogues follows that described previously (*19*) and includes the following ligands: D-myo-Inositol (1,4,5)-trisphosphate [$I(1,4,5)P_3$] (Sigma Aldrich, I 9766), the soluble headgroup for PI(4,5)-P_2, was used as an easily accessible ligand with established affinity and D-myo-inositol [myoI] (Sigma Aldrich, I 5125), containing only the inositol ring with no phosphates, was used as a negative control. Specificity was tested by varying the position and number of phosphates located on the inositol ring, as illustrated in Figure 1, including D-myo-inositol (1)-monophosphate [myoI-(1)P], D-myo-inositol (1,4)-bisphosphate [myoI-$(1,4)P_2$], and D-myo-inositol (4,5)-bisphosphate [myoI-$(4,5)P_2$](Sigma Aldrich, I 2523, I 0510, I 3264, respectively). A soluble $PI(4,5)P_2$ analogue, dibutyryl-phosphatidylinositol (4,5)-bisphosphate [dibutyryl-PI(4,5)-P_2] (Echelon Biosciences Inc., P 4504) was also used. However, due to its more limited solubility, dibutyryl-PI-$(4,5)P_2$ titrations ranged only from 0 to 3.5 mM.

NMR Experiments. HSQC-based titration experiments for pH studies and determination of chemical shift perturbations with samples containing myoI, $I(1,4,5)P_3$, and dibutyryl-PI-$(4,5)P_2$ were performed at 298 K on a Varian 800 MHz spectrometer (Varian Inc, Palo Alto, CA). Samples containing myoI-(1)P, myoI-$(1,4)P_2$, and myoI-$(4,5)P_2$ were collected on a Varian 600 MHz Spectrometer at 298 K using a *Z*-gradient triple-resonance Chili probe for enhancement of

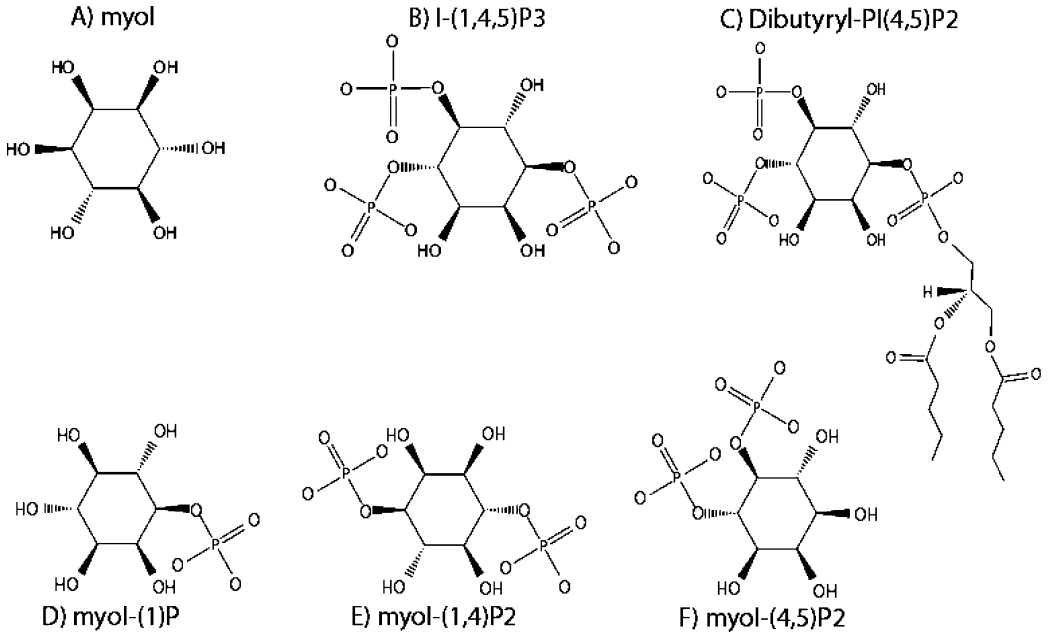

FIGURE 1: Ligands used in phosphoinositide binding studies with Arf1·GDP included (A) D-myo-inositol, containing only the inositol ring with no phosphates, (B) D-myo-inositol (1,4,5)-trisphosphate, the soluble headgroup for PI(4,5)P_2, (C) dibutyryl-PI(4,5)P_2, a short acyl-chain, soluble mimic for PI(4,5)P_2, (D) D-myo-inositol (1)-monophosphate, (E) D-myo-inositol (1,4)-bisphosphate, and (F) D-myo-inositol (4,5)-bisphosphate.

signal-to-noise (Varian Inc, Palo Alto, CA). Average data collection for the $^1H-^{15}N$ HSQC experiments included 2048 t_2 points and 128 t_1 points, which were subsequently modified with linear prediction and zero filling to 4096 and 512 points, respectively. Each spectrum required approximately 1 h. All data processing was performed with the NMRpipe/NMRdraw and NMRview packages (*20*, *21*).

The ^{31}P spectra used for analysis of nucleotide content were collected on a Mercury 300 MHz spectrometer with a Nalorac 4 nucleus probe using standard 1 D experiments having proton decoupling only during acquisition. Relatively long recycle times of 2 s were selected to minimize variations in peak intensities due to differential spin relaxation. ^{31}P chemical shifts were externally referenced to 85% phosphoric acid and internally referenced to 10 mM inorganic phosphate present in the sample buffer (pH 7.0).

$^1H-^{15}N$ Cleanex HSQC experiments were used to identify amide protons that rapidly exchange with protons from water in Arf1·GDP samples. Experiments were adapted from a previously described pulse sequence (*16*) and conducted on samples made at 0.5 mM protein in phosphate buffer. Data collection for the Cleanex $^1H-^{15}N$ HSQC experiments included 2048 t_2 points and 128 t_1 points subsequently extended with linear prediction and zero filling to 4096 and 512 points, respectively. Each spectrum required approximately 16 h.

$^1H-^{15}N$ HSQC-based surface accessibility experiments were run on Arf1·GDP (0.5 mM) with and without the presence of the paramagnetic spin probe TEMPOL (50 mM, 4-hydroxy-2,2,6,6-tetramethyl-piperidine-1-oxyl; Sigma Chemical Co.) to topologically map the solvent-exposed molecular surface both with and without the putative ligand (dibutyryl-PI(4,5)P_2). Data collection for the $^1H-^{15}N$ HSQC experiments included 2048 t_2 points and 128 t_1 points subsequently extended with linear prediction and zero filling to 4096 and 512 points, respectively. Each spectrum required approximately 4 h.

Determination of Dissociation Constants. Quantitation of perturbations seen at each titration point was achieved using eq 1, which takes the difference in chemical shifts and scales them with respect to the relative ranges of the chemical shift variation observed at saturation. Dissociation constants were extracted using a Tcl/Tk-based NMRview module, available upon request from Kevin Gardner (www.freedom7.swmed.edu).

$$\delta_{^1H^{15}N} = \frac{\sum(\delta_i)}{\delta_{i(\max)}} \quad (1)$$

The extraction of K_d values is based on fitting theoretical curves, generated using eq 2, where the value L is ligand concentration, P_T is the total protein concentration, K_d is the equilibrium dissociation constant, $\Delta\delta$ is the combined chemical shift change ($\delta_{^1H^{15}N}$) at a particular ligand concentration, and $\Delta\delta_{max}$ is the chemical shift change at saturation.

$$\Delta\delta = \frac{\Delta\delta_{\max}\{(L + P_T + K_d) - [(L + P_T + K_d)^2 - (4LP_T)]^{1/2}\}}{[2P_T]} \quad (2)$$

To improve the quality of fit, chemical shift values obtained from nine residues showing a substantial degree of chemical shift variation as a result of ligand addition (F5, A6, K10, L12, F13, G14, K16, R178, and K181) were scaled by chemical shift deviations seen at saturation and combined to produce a single titration curve. This presumes that all shifts arise from a single binding event, and to support this assumption, binding curves for individual residues showing large shift deviations from different regions of the protein were examined. They showed no significant deviations from the averaged curve. Moreover, the curves agree with a stoichiometry of 1:1 indicating no competition between different sites with similar binding constants.

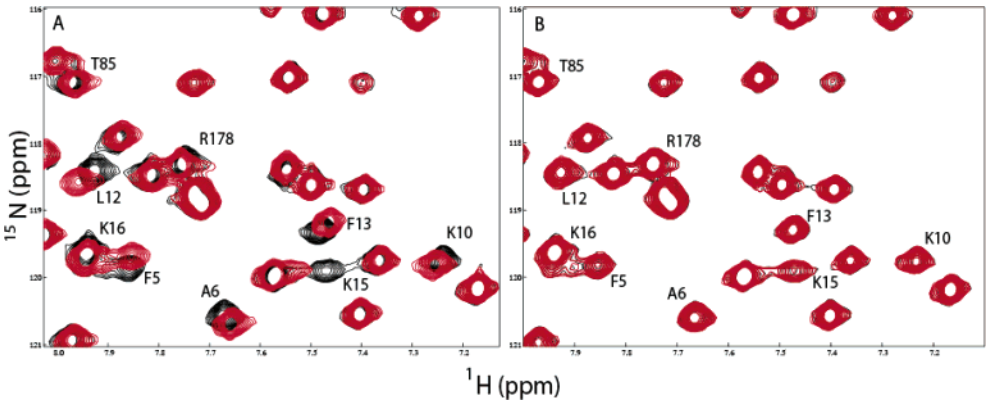

FIGURE 2: Section of an HSQC spectrum collected on 0.5 mM Arf1·GDP in 10 mM potassium phosphate (pH 7.0), 1 mM $MgCl_2$, 1 mM GDP, and 100 mM NaCl. Shown in black are peaks in the absence of ligand, and shown in red are peaks in the presence of ligand, (A) 8.0 mM I(1,4,5)P3 and (B) 8.0 mM myoI. Peaks showing chemical shift variation as a result of ligand addition are labeled with residue number and amino acid type for those residues assigned. All spectra were recorded at 298 K with a proton resonance frequency of 800 MHz, as described under Materials and Methods.

Ideally, the presence of ligand is the only contributor to chemical shift changes. However, some of the residues monitored also showed slight alterations in chemical shift owing to small changes in pH as a result of ligand addition. We attempted to remove pH contributions as follows. First, a separate pH titration was conducted. Second, during ligand titrations, pH changes were monitored using the chemical shift variation of H146, a residue shown to be very sensitive to local alterations in pH and being well removed from sites showing ligand binding effects. Finally, a pH contribution to chemical shifts of other residues was calculated by scaling the H146 shift at a ligand titration point by the ratio of the pH shift for each residue to the pH shift for H146 seen in the pH titration. The resulting chemical shift value (in ppm) for each residue was subsequently subtracted from the observed chemical shift deviation seen at each point in the ligand titration. All chemical shift deviations are represented on a normalized scale (0 to 1) as fractional shifts observed.

Quantitation of Paramagnetic Attenuation. As previously reported (*22*, *23*), paramagnetic effects were measured by comparing autoscaled cross-peak attenuation values (A_i), defined as

$$A_i = [2 - (v_{ip}/v_{id})] \quad (3)$$

with eq 3 being the individual deviations from the average of the cross-peak autoscaled volumes, $v_{ip,d,}$ the latter being defined as

$$v_{ip,d} = V_{ip,d}/[(1/n)(\sum_i V_{ip,d})] \quad (4)$$

where n is the number of measured cross-peak volumes and V_{id} and V_{ip} are the protein individual cross-peak volumes in the absence and presence of the spin probe, respectively. The individual A_i's were then plotted as a function of protein primary sequence. Values lying above or below the average attenuation level [set at 1, since $(\sum v_{ip,d}/n) = 1$] correspond to high or low spin probe accessibility, respectively. To better represent the surface-exposed residues, values lying above 1.2 were color-coded and superimposed on a three-dimensional surface plot of Arf1.

RESULTS

Phosphoinositide Binding. When the HSQC spectra obtained for Arf1·GDP in the presence (8 mM) and absence of I(1,4,5)P_3 were overlayed, distinct variations between the two states were readily observed, as shown in Figure 2A. These variations were absent from samples of Arf1·GDP containing D-myo-inositol, the core of I(1,4,5)P_3 lacking the phosphates, at the same concentration (Figure 2B). This serves as a control that assigns shifts seen with I(1,4,5)P_3 to specific interactions with phosphorylated inositols. The selective perturbation of chemical shifts shown in this segment of the HSQC spectra is for residues found in the positive patch on Arf1 or for amino acids comprising the amino-terminal helix (F5, A6, L12, F13, and K15).

A more complete detailing of resonances perturbed in response to the addition of a number of different phosphoinositides to Arf1 is shown in Figure 3. Here, limiting shifts in the ^{1}H and ^{15}N dimensions are plotted, weighting shifts by the ratio of observed sweep widths for ^{1}H and ^{15}N to remove bias as a result of the greater sensitivity of ^{15}N shifts (in ppm) to small conformational changes. The horizontal blue line at 0.02 ppm denotes the standard deviation observed over all changes. It is apparent that upon addition of I(1,4,5)-P_3 to Arf1 (Figure 3E), selective perturbations of individual resonances occur and that many of these are repeated for some of the other ligands (Figure 3C,D). Although the number of significant chemical shift perturbations observed might seem larger than expected, most can be assigned to a small number of structural regions. These changes map to three regions, one within the N-terminal helix and loop (residues F5, A6, K10, F13, K15, K16, and R17), a second including the positive patch (positive residues K10, K15, K16, and K181 and their adjacent residues R17, N179, and Q180), and a third around the nucleotide binding region including the P-loop (residues D26, A28, and G29), helix A (residues Y35 and K36), and the G3 binding motif (residues K127, Q128, and N132). Outside of these three regions, minor, or more isolated, perturbations are observed in β strands running through the protein core and connecting the N-terminal helix with the nucleotide binding pocket; specifically, residues in β1 (19-RIL-21), the interswitch region involving β2 and β3 (I49, V53, Y58, N60, and V65), and a residue in switch 2 (G69) are perturbed. Residues R99 and D164, located in surface-exposed loops, also show some perturbation. Note that resonances for residues K30 and T31 of helix A undergo substantial line broadening as a result of I(1,4,5)P_3 binding, preventing the measurement of chemical

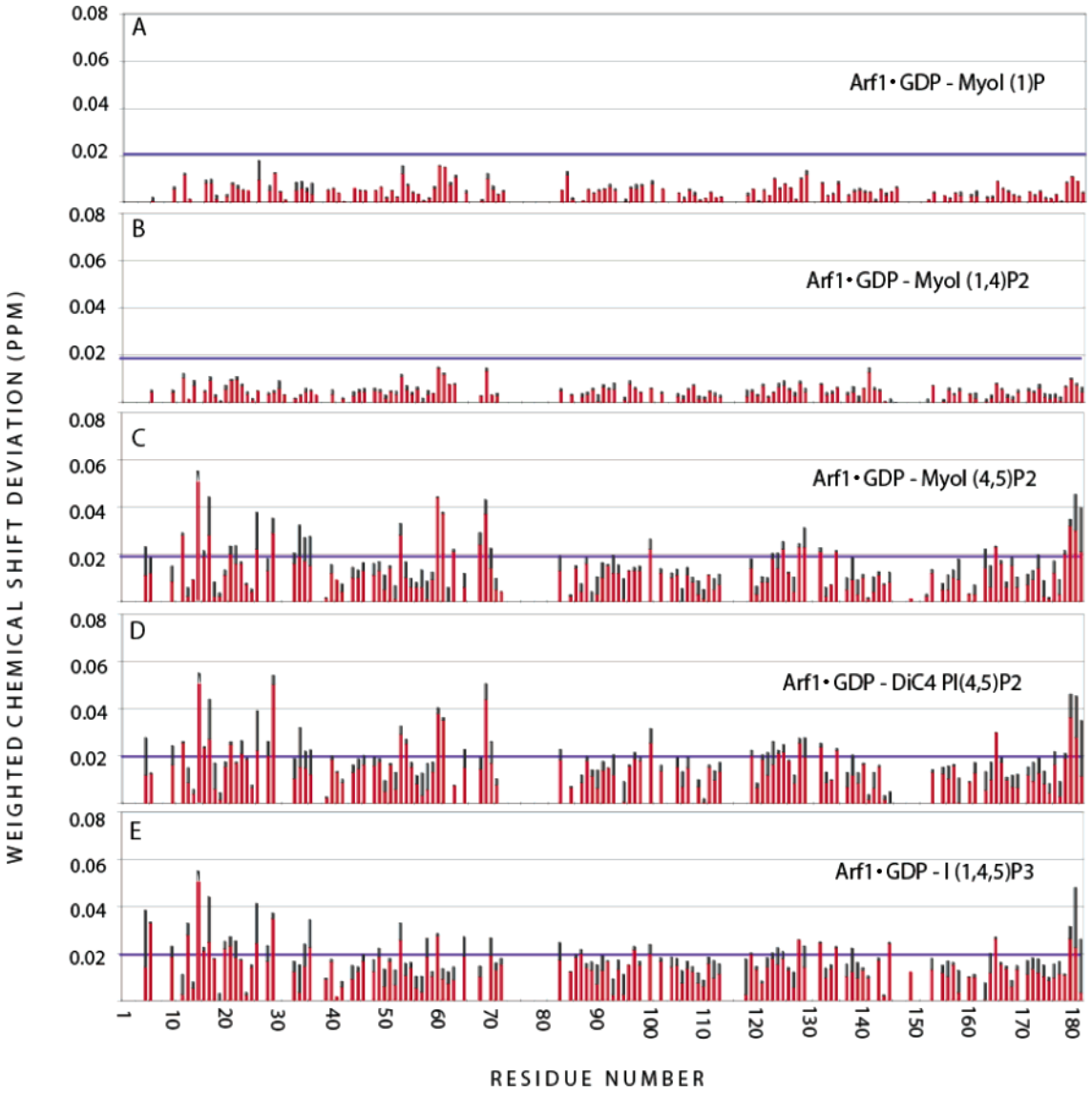

FIGURE 3: $^{15}N/^{1}H$ weighted chemical shift deviations in Arf1·GDP (0.5 mM) samples with various phosphoinositides are plotted as a function of residue number. Ligands used are as follows: (A) myoI-(1)P (8 mM), (B) myoI-(1,4)P_2 (8 mM), (C) myoI-(4,5)P_2 (8 mM), (D) dibutyryl-PI(4,5)P_2 (3 mM), and (E) I(1,4,5)P_3 (8 mM). Contributions to chemical shift variation from the ^{1}H dimension are shown in red with ^{15}N-specific contributions represented in gray. All values are shown as the overall magnitude of the deviation observed. Values above one average standard deviation are found above the horizontal blue line at 0.02 ppm.

shift offsets; they should also be included in the list of perturbed resonances.

Cell signaling by phosphatidylinositides is a very specific process that is controlled by addition of phosphate groups primarily to the 3, 4, and 5 positions on the inositol ring. Because charge effects make an important contribution to the protein interactions engaged by these multiply phosphorylated compounds, the stereochemistry of the phosphates is an important indicator of specificity. The importance of phosphate placement on the inositol ring was tested by examining chemical shift offsets in Arf1·GDP resonances in response to ligands that varied both in the position and number of phosphates on the inositol ring; these included myoI-(1)P, myoI-(1,4)P_2, and myoI-(4,5)P_2, as illustrated in Figure 1.

Chemical shift deviations observed for myoI-(1)P and myoI-(1,4)P_2 are small, even at the limiting concentrations of our studies (Figure 3A,B). This indicates weaker binding and shows that the simple presence of two phosphates on the inositol ring is not sufficient to cause the larger chemical shifts described above. However, myoI-(4,5)P_2 (Figure 3C) shows selective chemical shift perturbations very similar to those seen for I(1,4,5)P_3. These include residues in the surface-exposed positive patch on Arf1·GDP, as well as residues assigned to the N-terminal helix and the nucleotide binding loops. A few additional perturbations are found in switch 2 elements (V68 and G70), as well as helix A (L34). These observations suggest that the placement of the 5-phosphate or the vicinal (4,5)-bisphosphate combination is a critical element for binding and that I(1,4,5)P_3 and myoI-(4,5)P_2 are likely to share a common binding site.

Because the soluble I(1,4,5)P_3 and membrane-associated PI(4,5)P_2 each have signaling capabilities in cells, we wanted to assess the importance of the hydrophobic portion of the lipid in interactions with Arf1. A water-soluble, short acyl-chain analogue (dibutyryl-phosphatidylinositol (4,5)-bisphosphate [dibutyryl-PI(4,5)P_2]) was examined for its ability to bind Arf1·GDP (molecule diagrammed in Figure 1). A

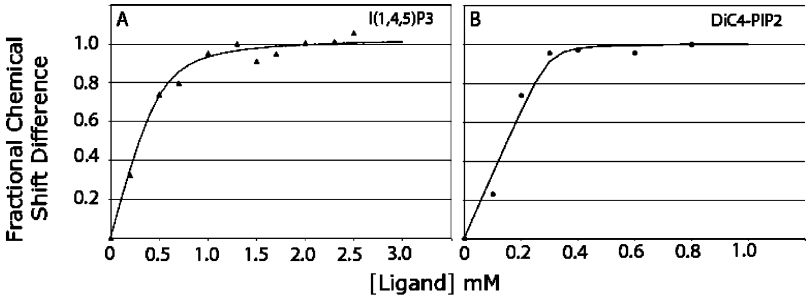

FIGURE 4: Quantitation of perturbations as a function of ligand concentration. HSQC spectra were obtained for samples containing Arf1·GDP (0.5 mM) with varying amounts of I(1,4,5)P_3 (A, ▲) or Arf1·GDP (0.3 mM) with varying amounts of dibutyryl-PI(4,5)P_2 (B, ●). Normalized deviations in chemical shifts observed for each point were obtained using eq 1 (see Materials and Methods). Dissociation constants were extracted using a Tcl/Tk-based NMRview module and eq 2 as described in Materials and Methods. A line simulated using the derived dissociation constant is included for comparison.

binding pattern again reminiscent of I(1,4,5)P_3 association was found (Figure 3D), suggesting that the polar headgroup remains involved in direct binding to Arf1 for all these ligands. However, as we illustrate below, the lipid portion appears to enhance binding.

Determination of Dissociation Constants. In select cases, it is possible to use the concentration-dependent changes in chemical shifts to determine binding constants for ligands. To do this, chemical shift differences for I(1,4,5)P_3 and dibutyryl-PI(4,5)P_2 upon addition of ligand were plotted and fit using eqs 1 and 2 (see Materials and Methods) over the titration range 0−8 and 0−1.2 mM, respectively (Figure 4). Normalized deviations in chemical shift are plotted for each titration point, as described in the Materials and Methods section. The observed chemical shifts for I(1,4,5)P_3 clearly shift monotonically as a function of concentration (Figure 4A), indicating a ligand that is in fast exchange on the NMR time scale. Shifts also cease to deviate at high ligand concentrations (above 1.25 mM), indicating an ability to saturate the binding site. This behavior allows an accurate determination of the dissociation constant ($K_{D(apparent)} = 56 \pm 15\ \mu$M). Titration with dibutyryl-PI(4,5)P_2, while showing an ability to saturate the binding site (limiting concentration of 0.4 mM, Figure 4B) is more indicative of a ligand that is in slow exchange on the NMR time scale. Peaks from spectra below 0.3 mM show broadening that can be interpreted as superposition of pairs of poorly resolved peaks. Changes in intensity distribution between pairs gives the appearance of a change in chemical shift. While this behavior prohibits the accurate determination of the dissociation constant, an upper limit can be estimated from the saturation point (KD < 10 μM).

For myoI-(1)P and myoI-(1,4)P_2 significant shifts were not observed even at high concentrations. This is indicative of very weak binding (K_D > 10 mM) or the lack of an ability to induce shift perturbations. MyoI-(4,5)P_2 produced limiting shifts comparable to I(1,4,5)P_3, but due to the small number of titration points collected with limited quantity ligand available to us, a quantitative determination of binding was not attempted. However, the fact that a limiting shift was reached near 2.0 mM allows us to set an upper limit for the dissociation constant of 500 μM. Hence myoI-(4,5)P_2 binds with an affinity noticeably lower than I(1,4,5)P_3 and dibutyryl-PI(4,5)P_2 binds with an affinity considerably higher than I(1,4,5)P_3. Thus, although neither the glycerol nor the acyl-chains are required for interaction with Arf1, their presence increases the affinity for Arf1, either through direct contacts with the protein or indirectly through effects on the structure of the inositol and associated phosphates.

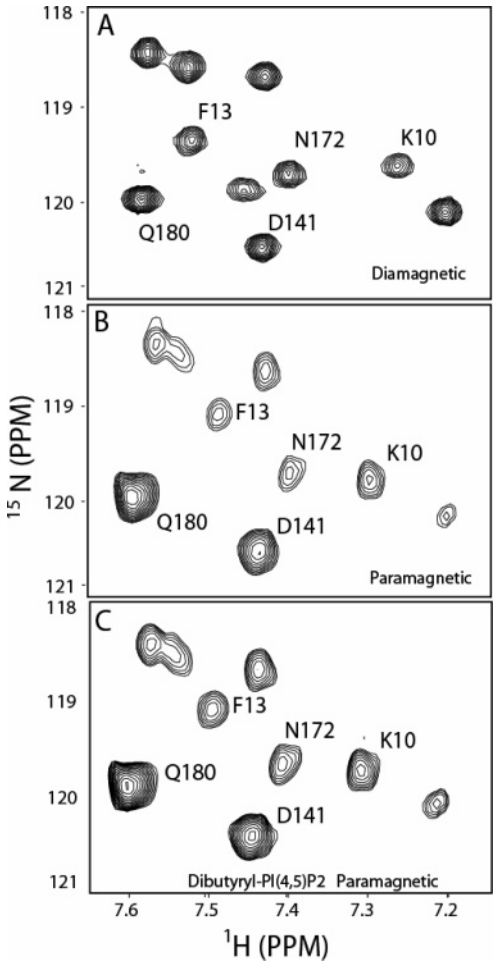

FIGURE 5: Section of an HSQC spectrum collected on 0.5 mM Arf1·GDP in (A) 10 mM potassium phosphate (pH 7.0), 100 mM NaCl, 1 mM $MgCl_2$, and 1 mM GDP, (B) the same buffer with the addition of 50 mM TEMPOL, and (C) the same buffer upon addition of 3.0 mM dibutyryl-PI(4,5)P_2 and 50 mM TEMPOL. Representative peaks showing paramagnetic attenuation as a result of TEMPOL accessibility are labeled with residue number and amino acid type. All spectra were recorded at 298 K with a proton resonance frequency of 600 MHz, as described under Materials and Methods.

Binding Site Verification. In cases where selective perturbations are seen upon ligand addition (myoI-(4,5)P_2, dibutyryl-PI(4,5)P_2, and I(1,4,5)P_3), the perturbations occur in at least three regions of the protein. Because chemical

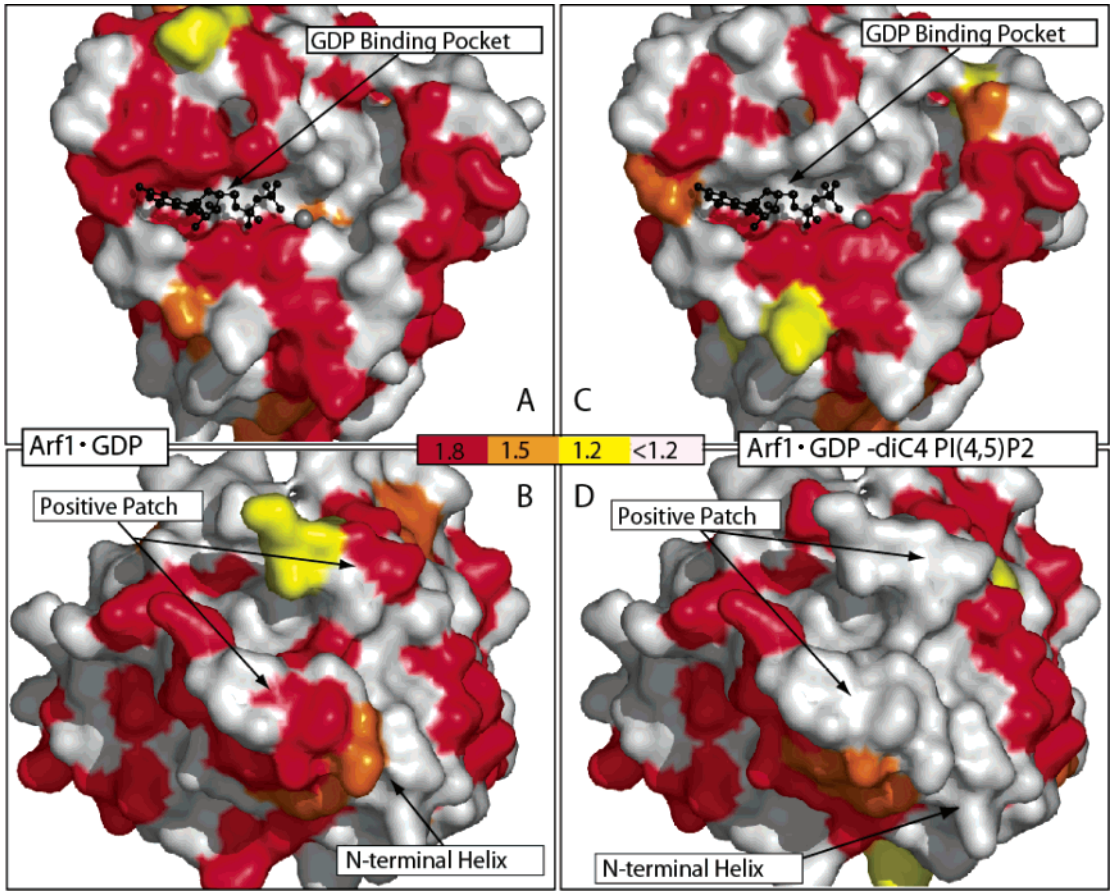

FIGURE 6: Arf1·GDP surface accessibility map derived from TEMPOL spin probe attenuation observed in both the absence (panels A and B, labeled Arf1·GDP) and presence (panels C and D, labeled Arf1·GDP −diC4 PI(4,5)P_2) of dibutyryl-PI(4,5)P_2 (3 mM). Cross-peak attenuations in the nucleotide binding face (panels A and C) and the surface-exposed positive patch (panels B and D) are superimposed onto a three-dimensional surface model of Arf1. The A−B and C−D pairs are related by approximately a 180° rotation. The cross-peak attenuations observed are scaled to a maximum value of 2 with values lying above 1 corresponding to increased spin-probe accessibility levels. The representative surface maps are color-coded to illustrate the degree of paramagnetic attenuation (red values 1.8 or greater, orange 1.5−1.8, yellow 1.2−1.5, and gray less than 1.2].

shift perturbations can occur at remote sites due to allosteric propagation, it is difficult to assess which region of the protein is contacting the ligand directly. It is therefore important, whenever possible, to supplement chemical shift data with other information to determine the direct site of ligand interaction on the protein surface. One of the additional experiments that can supplement chemical shift offsets is perturbation of relaxation times for surface-exposed amide proton−amide nitrogen cross-peaks by water-soluble paramagnetic species (*14*, *22*). By monitoring cross-peak attenuations in HSQC spectra upon addition of the stable free radical TEMPOL (50 mM) to the solvent (*22*), topological mapping of the Arf1 protein surface was achieved. Cross-peaks most attenuated are those derived from surface-exposed residues. An example of the data acquired is illustrated in Figure 5. The variation in cross-peak attenuation levels between spectra recorded in the presence and in the absence of small ligand molecules can also show regions of protection afforded to the molecular surface as a result of ligand addition. Because the origin of these differences is largely steric exclusion and is very different in origin from that of chemical shift perturbations, the data nicely complement the chemical shift information.

Figure 6A,B shows the results in the absence of ligand mapped onto a surface representation of the protein (PDB code 1HUR) for both the nucleotide binding face (A) and surface-exposed positive patch (B). The cross-peak attenuations observed are scaled, as described in the Materials and Methods section, to a maximum value of 2 with values lying above 1 corresponding to increased spin-probe accessibility levels. The representative surface maps are color-coded to illustrate the degree of paramagnetic attenuation (red having values 1.8 or greater, orange 1.5, yellow 1.2, and gray <1.2]. Addition of the ligand (dibutyryl-PI(4,5)P_2) changes the TEMPOL-derived surface accessibility patterns, as shown in Figure 6C,D. Extensive changes are seen near the positive patch upon ligand addition; specifically, a decrease in surface accessibility of residues K10, L12, F13, and 178-RNQK-181 is seen. Alterations to the nucleotide-binding region were also seen upon ligand addition, specifically in residues V123, K127, and D129, but because these changes are fewer in number and lie along one face of the bound nucleotide, they were deemed much less likely to result from direct interaction with the ligand. These data lead us to conclude that the chemical shift perturbations observed for resonances found in and around the positive patch result from direct contact with the ligand and those observed for resonances from the nucleotide binding site, or intervening structural elements, are more likely a secondary effect of ligand binding observed through allosteric propagation.

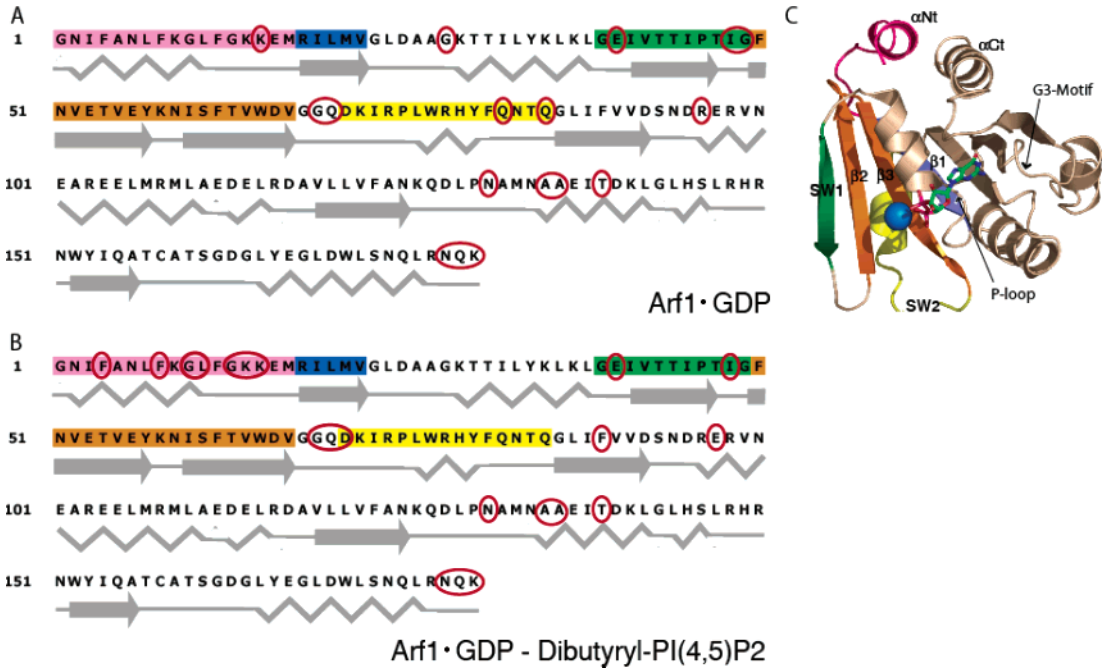

FIGURE 7: $^{1}H-^{15}N$ Cleanex HSQC comparisons showing areas of rapid exchange between water and amide protons of Arf1·GDP (A) and Arf1·GDP−dibutyryl-PI(4,5)P_2 (B). Secondary structural elements are shown as a cartoon beneath the protein sequence, shown using the single letter amino acid code. Resonances evident in a $^{1}H-^{15}N$ Cleanex HSQC experiment are circled in red. To relate these regions of enhanced exchange to a three-dimensional model, the structure of Arf1·GDP is shown as a cartoon representation (C) color-coded as follows: N-terminal α helix, magenta; switch 1, green; interswitch region, orange; switch 2, yellow.

Conformational Destabilization upon Phosphoinositide Binding. It has been previously suggested that PI(4,5)P_2 binding might stimulate the release of bound GDP from membrane-associated Arf1 (*2*, *5*, *9*). To address the potential for conformational destabilization in Arf1·GDP seen in complex with the phosphoinositides used in our study, we compared the changes in energetic properties of the protein between ligand-bound and unbound states, as assessed through measurement of amide proton exchange rates. The amide group is assumed to be in rapid equilibrium between protected and exposed forms with base-catalyzed exchange of the amide proton for a water proton in the open form being the rate-limiting step (*15*). Under these conditions, increases in rates of exchange primarily reflect destabilization of protected forms and a shift in equilibrium toward conformations that expose amide protons to solvent. When rates of interest are moderately fast, modulation in HSQC peak intensities can be observed using experiments in which water protons are labeled by saturation or inversion of magnetization. Differences between spectra with water magnetization perturbed and not perturbed highlight cross-peaks belonging to amides experiencing rapid proton exchange and an ability to acquire magnetization from water protons. The CLEANEX HSQC is an experiment of this class that has been designed to minimize artifacts from inadvertent perturbation of α protons underlying the water resonance (*16*).

CLEANEX HSQC data for Arf1·GDP in the absence and presence of dibutyryl-PI(4,5)P_2 are summarized in Figure 7, panels A and B, respectively. Here residues having amides showing exchange sufficiently rapid to acquire magnetization from water protons are circled. There are more such residues in the ligand-bound case (Figure 7B), indicating an increase in exposed residues or destabilization of secondary structure elements that protect amide protons from exchange in unbound Arf1·GDP (Figure 7A). As expected, the majority of rapidly exchanging amides are in loops between secondary structural elements in both ligand-free and -bound states. Major differences seen upon ligand binding occur in the gain of some rapidly exchanging elements in the N-terminal helix of Arf1·GDP (Figure 7B), along with elements in switch 2 (e.g., D72), and the loss of rapidly exchanging elements in the P-loop (G29, Figure 7A), the loop succeeding switch 1 (G50), and the loop from 83 to 85 at the end of the switch 2 helix.

Because a number of changes in amide exchange rates involve loops near the nucleotide binding site, we wanted to examine more closely the specific effects on the bound nucleotide that accompanied ligand binding. This was addressed by observing the naturally occurring ^{31}P resonances attached to the guanine base in both free and bound GDP in the Arf1·GDP−dibutyryl-PI(4,5)P_2 complex. GDP has distinctive ^{31}P chemical shift values for the β phosphorus in the bound and free states, allowing for a direct detection of bound nucleotide. ^{31}P spectra were recorded from Arf1·GDP in the absence and presence of dibutyryl-PI(4,5)P_2 (Figure 8) The spectra show an overall retention of the nucleotide within the binding pocket of Arf1 in solution. However, comparing integrated peak intensities of ^{31}P peaks observed in the spectra from GDP to internal standards indicates a change in the binding equilibrium favoring nucleotide release upon ligand addition. The change in the ratio of free to bound β phosphate intensities is from 0.11 to 0.26. It was seen that when dibutyryl-PI(4,5)P_2 is bound there are energetic changes in protein elements near the nucleotide binding site and there appears to be a coupled shift toward a lower binding constant for GDP and consequent release of the nucleotide.

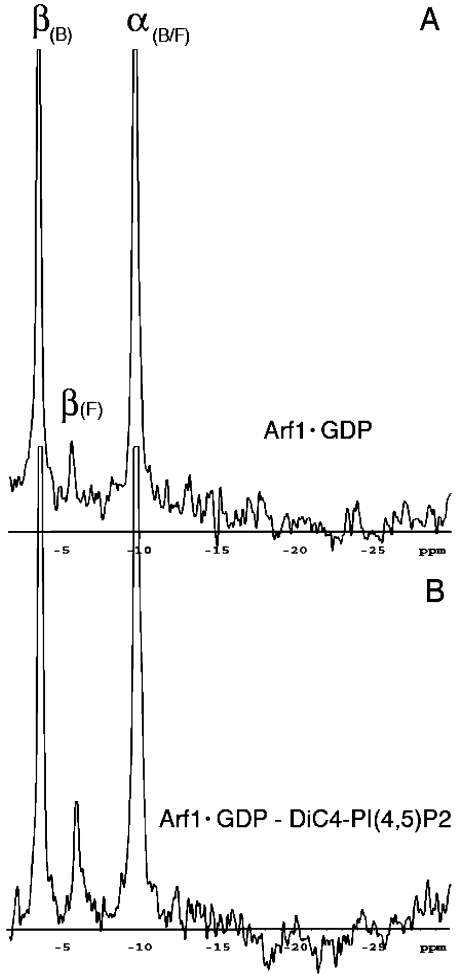

FIGURE 8: ^{31}P spectra recorded on Arf1·GDP (0.5 mM) in the absence (A) and presence (B) of dibutyryl-PI(4,5)P_2 (3 mM). Phosphates observed are labeled by phosphate type (α/β) along with bound state (F = free or B = bound). Note that α resonances are overlapped between free and bound GDP. Integration of peak intensities shows as an increase in the amount of the free β phosphate from GDP upon ligand binding (the ratio of β_F/β_B changes from 0.11 to 0.26). All spectra were recorded with a proton resonance frequency of 300 MHz at 298 K.

DISCUSSION

The localized production and sensing of phosphorylated forms of phosphatidylinositols is an integral part of Arf biology. This is both because activated Arfs can recruit and directly activate the enzymes (PI 4-kinase and PI(4)P 5-kinase) controlling the formation of these signaling lipids and because the product of these kinases (PI(4,5)P_2) is a required cofactor in both Arf-dependent phospholipase D and Arf GAP activities and assists in the recruitment to membranes of a subset of Arf GEFs. A further complication to the development of molecular models of Arf action stems from the observation that PI(4,5)P_2 can bind directly to Arf1 and alter its affinity for guanine nucleotides (*9*, *10*). Several studies have suggested structural changes involved in the activation of Arf proteins and in their binding to Arf GEFs. These include substantial changes to the amphipathic N-terminal helix, nucleotide-binding pocket, interswitch region, and connecting strands (*1*, *24*). We sought additional structural evidence to test the hypothesis that binding to phosphatidylinositols may play a facilitative role in the activation of Arf1. Using a number of NMR techniques, we document here specificity in the binding to different phosphatidylinositides, chemical shift changes in specific positively charged residues on one surface of Arf1 that we propose to result from direct interaction with the ligand, and allosteric changes in the nucleotide binding site that accompany ligand binding, all of which support the conclusion that binding to PI(4,5)P_2 can promote the nucleotide exchange process and facilitate activation of Arfs.

Tests of specificity for the ability to induce chemical shift changes in Arf1 revealed a dependence on vicinal phosphates on the inositol ring (see Figure 3). Nonspecific charge effects are not viewed as a viable explanation for the changes observed here because myo-I(1,4)P_2 was without effect while myo-I(4,5)P_2 was comparable to perturbations induced by I(1,4,5)P_3 or dibutyryl-PI(4,5)P_2. The concentration dependence in chemical shifts induced by I(1,4,5)P_3 was then used to determine an apparent binding constant, and the value obtained ($K_{D(apparent)} = 56 \pm 15$ μM) was comparable to that determined previously for the binding of Arf1·GTP to PI(4,5)P_2 in Triton X-100 micelles (45 $\pm$13 μM, *5*). In contrast, we found that the addition of even very short acyl chains (dibutyryl-PI(4,5)P_2) increased the affinity to give a dissociation constant below 10 μM. This increase in affinity may result either from an induced alteration in the structure or charge distribution of the inositol and associated phosphates to give a form that binds better to Arf1 or from a direct involvement of the glycerol or one or both butyrates in binding to the protein. While the similarity in binding properties of Arf1 observed in solution and in a detergent micelle (*5*) suggest an ability to extrapolate to a membrane environment, it is important to point out that we still do not know the affinity of any Arf for PI(4,5)P_2 in the context of a biological membrane. However, on the basis of the dibutyryl-PI(4,5)P_2 data, we can speculate that the dissociation constant is below 10 μM and is in the physiological range. Our data were all collected for Arf1 in solution, but with the use of membrane mimics (e.g., bicelles), we should be able to extend the use of NMR techniques to an even better approximation of the physiologically important Arf−lipid interactions.

Structural consequences of ligand binding extend far beyond the actual phosphoinositide-binding patch (shown as a surface plot in Figure 9A with perturbed resonances highlighted in red). Assigned resonances comprising the N-terminal helix (Figure 9B) and the nucleotide-binding pocket (αA/P-loop and G3 motif, Figure 9C) are also perturbed, indicating a change in the local electronic environment around those residues. CLEANEX HSQC experiments show changes in stability of secondary structural elements of several of these segments supporting a propagated change in structure to the N-terminal helix and the nucleotide-binding site. Nucleotide destabilization and subsequent release in native environments that contain phosphoinositides have been described in the literature (*9*, *10*, *25*), and our study has shown that this extends to solution conditions where a change in the equilibrium of GDP binding occurs as evidenced in ^{31}P experiments. The stabilization changes in protein structural elements and these changes in nucleotide binding properties are likely to be coupled.

On the basis of our observations, Arf1·GDP is proposed to associate with PI(4,5)P_2 at the membrane, allowing for the local structural modifications required for nucleotide

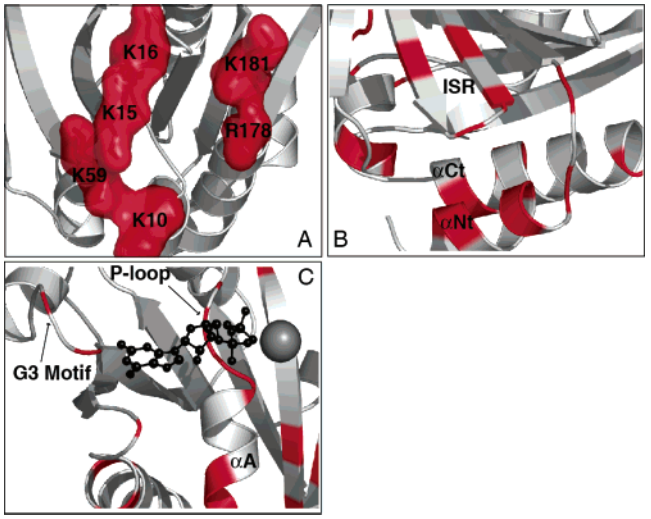

FIGURE 9: Crystal structure of Arf1·GDP highlighting regions affected by phosphoinositide binding: (A) the solvent-exposed positive patch on Arf1·GDP; (B) the interswitch region (ISR), the N-terminal helix (αNt), and the C-terminal helix (αCt); (**C**) the nucleotide binding pocket (P-loop, αA, and G3 motif). Assigned residues showing chemical shift perturbations in HSQC titrations are colored red.

destabilization and possibly alteration in the position and stability of the N-terminal helix. Disruption of the N-terminal helix upon membrane or Arf-GEF association can be substantiated by comparing crystal structures of specific Arf1 variants; particularly comparing Arf1, deleted of its N-terminal helix, associated with its corresponding GEF and bound to either GDP or GTP (*1*, *24*) with those of Arf1·GDP alone (*4*, *26*). Such a comparison reveals that Arf1·GDP assumes a conformation that is unable to fit into the binding pocket of its corresponding GEF in solution (*2*, *27*, *28*). This association would ultimately require the removal of the N-terminal helix from its binding cleft in inactive Arf and a displacement of β strands within the protein core. Because the substantial degree of conformational change needed for GEF-association would be energetically unfavorable in solution, Arf1 is suggested to first interact with the membrane surface, potentially initiating the needed conformational changes prior to association with its GEF. Data presented here suggest that specific interactions with membrane associated $PI(4,5)P_2$ can contribute to the needed conformational changes. Further structural studies on Arf1·GDP−Arf1GEF complexes involving membrane-imbedded $PI(4,5)P_2$ are needed to verify this suggestion.

ACKNOWLEDGMENT

We would like to thank Dr. Gregory Wylie, Anita Kishore, and Dr. Michael Ford for their help throughout this project.

REFERENCES

1. Renault, L., Guibert, B., and Cherfils, J. (2003) Structural Snapshots of the mechanism and inhibition of a guanine nucleotide exchange factor, *Nature 426*, 525−530.
2. Paris, S., Beraud-Dufor, S., Robineau, S., Bigay, J., Antonny, B., Chabre, M., and Chardin, P. (1997) Role of Protein-Phospholipid Interactions in the Activation of ARF1 by the Guanine Nucleotide Exchange Factor Arno, *J. Biol. Chem. 272*, 22221−22226.
3. Macia, E., Paris, S., and Chabre, M. (2000) Binding of the PH and Polybasic C-terminal Domains of ARNO to Phosphoinositides and to Acidic Phospholipids, *Biochemistry 39*, 5893−5901.
4. Amor, J. C., Harrison, D. H., Kahn, R. A., and Ringe, D. (1994) Structure of the human ADP-ribosylation factor 1 complexed with GDP, *Nature 372*, 704−708.
5. Randazzo, P. (1997) Functional interaction of ADP-ribosyaltion factor 1 with phosphatidylinositol 4,5-bisphosphate, *J. Biol. Chem. 272*, 7688−7692.
6. Kahn, R. A., Yucel, J. K., and Malhotra, V. (1993) ARF signaling: a potential role for phospholipase D in membrane traffic, *Cell 75*, 1045−1048.
7. Martin, A., Brown, F. D., Hodgkin, M. N., Bradwell, A. J., Cook, S. J., Hart, M., and Wakelam, M. J. (1996) Activation of phospholipase D and phosphatidylinositol 4-phosphate 5-kinase in HL60 membranes is mediated by endogenous Arf but not Rho, *J. Biol. Chem. 271*, 17397−17403.
8. Randazzo, P. A., and Kahn, R. A. (1994) GTP hydrolysis by ADP-ribosylation factor is dependent on both an ADP- ribosylation factor GTPase-activating protein and acid phospholipids, *J. Biol. Chem. 269*, 10758−10763.
9. Terui, T., Kahn, R. A., and Randazzo, P. A. (1994) Effects of acid phospholipids on nucleotide exchange properties of ADP-ribosylation factor 1. Evidence for specific interaction with phosphatidylinositol 4,5-bisphosphate, *J. Biol. Chem. 269*, 28130−28135.
10. Kahn, R. A., Terui, T., and Randazzo, P. A. (1996) Effects of acid phospholipids on ARF activities: potential roles in membrane traffic *J. Lipid Mediators Cell Signalling 14*, 209−214.
11. Kay, L. E., Keifer, P., and Saarinen, T. (1992) Pure Absorption Gradient Enhanced Heteronuclear Single Quantum Coherence Correlation Spectroscopy with Improved Sensitivity, *J. Am. Chem. Soc. 114*, 10663−10665.
12. Stonehouse, J., Shaw, G. L., Keeler, J., and Laue, E. D. (1994) Minimizing Sensitivity Losses in Gradient-Selected N-15-H-1 HSQC Spectra of Proteins, *J. Magn. Res. A. 107*, 178−184.
13. Amor, J., Seidel, R., Tian, F., Kahn, R., and Prestegard, J. (2002) Letter to the Editor: H-1, N-15 and C-13 assignments of full length human ADP Ribosylation Factor 1 (ARF1) using triple resonance connectivities and dipolar couplings, *J. Biomol. NMR 23*, 253−254.
14. Niccolai, N., Ciutti, A., Spiga, O., Scarselli, M., Bernini, A., Bracci, L., Maro, D. D., Dalvit, C., Molinari, H., Esposito, G., and Temussi, P. (2001) NMR Studies of Protein Surface Accessibility, *J. Biol. Chem. 276*, 42455−42461.
15. Dempsey, C. E. (2001) Hydrogen Exchange in peptides and proteins using NMR spectroscopy, *Prog. NMR Spectrosc. 39*, 135−170.
16. Hwang, T.-L., Mori, S., Shaka, A. J., and Zijl, P. C. M. v. (1997) Application of Phase Modulated CLEAN Chemical EXchange Spectroscopy (CLEANEX-PM) to Detect Water-Protein Proton Exchange and Intermolecular NOEs, *J. Am. Chem. Soc. 119*, 6203−6204.
17. Randazzo, P. A., and Kahn, R. A. (1995) Myristoylation and ADP-ribosylation factor function, *Methods Enzymol. 250*, 394−405.
18. Neidhart, F. C., Bloch, P. L., and Smith, D. F. (1974) Culture Medium for Enterobacteria, *J. Bacteriol. 119*, 736.
19. Hyvonen, M., Macias, M. J., Nilges, M., Oschkinat, H., Saraste, M., and Wilmanns, M. (1995) Structure of the binding site for inositol phosphates in a PH domain, *EMBO J. 14*, 4676−4685.
20. Delaglio, F., Grzesiek, S., Vuister, G., Zhu, G., Pfeifer, J., and Bax, A. (1995) NMRPipe: a multidimensional spectral processing system based on UNIX pipes, *J. Biomol. NMR 6*, 277−293.
21. Johnson, B., and Blevins, R. (1994) NMRView - A Computer-Program for the Visualization and Analysis of NMR Data, *J. Biomol. NMR 4*, 603−614.
22. Scarselli, M., Bernini, A., Segoni, C., Molinari, H., Esposito, G., Lesk, A., Laschi, F., Temussi, P., and Niccolai, N. (1999) Tendamistat surface accessibilty to the TEMPOL paramagnetic probe, *J. Biomol. NMR 15*, 125−133.
23. Molinari, H., Esposito, G., Pegna, M., Ragona, L., Niccolai, N., and Zetta, L. (1997) Probing Protein structure by solvent Perturbation of NMR Spectra: The Surface Accessibility of bovine Pancreatic Trypsin Inhibitor, *Biophys. J. 73*, 382−396.
24. Goldberg, J. (1998) Structural basis for activation of ARF GTPase: mechanisms of guanine nucleotide exchange and GTP-myristoyl switching, *Cell 95*, 237−248.

25. Zheng, Y., Glaven, J. A., Wu, W. J., and Cerione, R. A. (1996) Phosphatidylinositol 4,5-bisphosphate provides an alternative to guanine nucleotide exchange factors by stimulating the dissociation of GDP from Cdc42Hs, *J. Biol. Chem. 271*, 23815−23819.
26. Greasley, S. E., Jhoti, H., Teahan, C., Solari, R., Fensome, A., Thomas, G. M., Cockcroft, S., and Bax, B. (1995) The structure of rat ADP-ribosylation factor-1 (ARF-1) complexed to GDP determined from two different crystal forms, *Nat. Struct. Biol. 2*, 797−806.
27. Beraud-Dufour, S., Paris, S., Chabre, M., and Antonny, B. (1999) Dual interaction of ADP Ribosylation Factor 1 with Sec7 domain and with lipid membranes during catalysis of guanine nucleotide exchange, *J. Biol. Chem. 274*, 37629−37636.
28. Franco, M., Chardin, P., Chabre, M., and Paris, S. (1996) Myristoylation-facilitated binding of the G protein ARF1GDP to membrane phospholipids is required for its activation by a soluble nucleotide exchange factor, *J. Biol. Chem. 271*, 1573−1578.

BI0490385